NAVAL POSTGRADUATE SCHOOL

MONTEREY, CALIFORNIA

THESIS

OPTICAL KINEMATICS OF WAVE-SWEPT SURGE CHANNEL RIP CURRENTS

by

Nicholas S. Patria

December 2018

Thesis Advisor: James H. MacMahan
Second Reader: Matthew K. Gough

THIS PAGE INTENTIONALLY LEFT BLANK

REPORT DOCUMENTATION PAGE			*Form Approved OMB No. 0704-0188*

1. AGENCY USE ONLY *(Leave blank)*	**2. REPORT DATE** December 2018	**3. REPORT TYPE AND DATES COVERED** Master's thesis

4. TITLE AND SUBTITLE OPTICAL KINEMATICS OF WAVE-SWEPT SURGE CHANNEL RIP CURRENTS	**5. FUNDING NUMBERS**
6. AUTHOR(S) Nicholas S. Patria	
7. PERFORMING ORGANIZATION NAME(S) AND ADDRESS(ES) Naval Postgraduate School Monterey, CA 93943-5000	**8. PERFORMING ORGANIZATION REPORT NUMBER**
9. SPONSORING / MONITORING AGENCY NAME(S) AND ADDRESS(ES) N/A	**10. SPONSORING / MONITORING AGENCY REPORT NUMBER**

11. SUPPLEMENTARY NOTES The views expressed in this thesis are those of the author and do not reflect the official policy or position of the Department of Defense or the U.S. Government.

12a. DISTRIBUTION / AVAILABILITY STATEMENT Approved for public release. Distribution is unlimited.	**12b. DISTRIBUTION CODE** A

13. ABSTRACT (maximum 200 words)

Aerial imagery of the rocky shoreline (RS) at Hopkins Marine Station in Pacific Grove, CA, was captured with an unmanned aerial vehicle. Imagery was georectified and post-processed to observe the surface flow of 2 persistent, stationary rip currents (rips) on the RS. Waves propagating toward the shoreline break as they interact with the irregular bathymetry. The collision of reflected waves in combination with a network of small feeder channels converge into a larger surge channel, directing a jet of water offshore. Breaking waves also create bubbles that inundate the shoreline with a dense bubble zone. Farther-extending bubbles within the rips were used to determine the cross-shore (CS) extent. Rip extents in channels 1 and 2 ranged between 14.3–49.2m and 8.8–33.1m. The respective mean extents were 33.1m and 18.1m. A dependence on wave height and tidal elevation is observed; as wave heights increase, the extent of the rips increases and, inversely, as tidal elevations decrease, extents increase. Slopes of ejected foam trajectories were measured for CS velocity. Calculated slopes show a velocity decay as the flow moves farther offshore. RS rips exhibit a direct offshore transport circulation. Drifters released from the shoreline immediately exited the surf zone and traveled along foam streaks, indicative of Lagrangian coherent structures. Maximum foam extents were observed at 154m, indicating surface material moving substantially offshore relative to the small surf zone.

14. SUBJECT TERMS wave-swept surge channel, rip currents, unmanned aerial vehicle, rocky shoreline, foam, aerial imagery	**15. NUMBER OF PAGES** 53
	16. PRICE CODE

17. SECURITY CLASSIFICATION OF REPORT	**18. SECURITY CLASSIFICATION OF THIS PAGE**	**19. SECURITY CLASSIFICATION OF ABSTRACT**	**20. LIMITATION OF ABSTRACT**
Unclassified	Unclassified	Unclassified	UU

NSN 7540-01-280-5500 Standard Form 298 (Rev. 2-89) Prescribed by ANSI Std. 239-18

THIS PAGE INTENTIONALLY LEFT BLANK

Approved for public release. Distribution is unlimited.

OPTICAL KINEMATICS OF WAVE-SWEPT SURGE CHANNEL RIP CURRENTS

Nicholas S. Patria
Lieutenant Commander, United States Navy
BS, Salisbury State University, 2008

Submitted in partial fulfillment of the
requirements for the degree of

MASTER OF SCIENCE IN METEOROLOGY AND PHYSICAL OCEANOGRAPHY

from the

NAVAL POSTGRADUATE SCHOOL
December 2018

Approved by: James H. MacMahan
Advisor

Matthew K. Gough
Second Reader

Peter C. Chu
Chair, Department of Oceanography

THIS PAGE INTENTIONALLY LEFT BLANK

ABSTRACT

Aerial imagery of the rocky shoreline (RS) at Hopkins Marine Station in Pacific Grove, CA, was captured with an unmanned aerial vehicle. Imagery was georectified and post-processed to observe the surface flow of 2 persistent, stationary rip currents (rips) on the RS. Waves propagating toward the shoreline break as they interact with the irregular bathymetry. The collision of reflected waves in combination with a network of small feeder channels converge into a larger surge channel, directing a jet of water offshore. Breaking waves also create bubbles that inundate the shoreline with a dense bubble zone. Farther-extending bubbles within the rips were used to determine the cross-shore (CS) extent. Rip extents in channels 1 and 2 ranged between 14.3–49.2m and 8.8–33.1m. The respective mean extents were 33.1m and 18.1m. A dependence on wave height and tidal elevation is observed; as wave heights increase, the extent of the rips increases and, inversely, as tidal elevations decrease, extents increase. Slopes of ejected foam trajectories were measured for CS velocity. Calculated slopes show a velocity decay as the flow moves farther offshore. RS rips exhibit a direct offshore transport circulation. Drifters released from the shoreline immediately exited the surf zone and traveled along foam streaks, indicative of Lagrangian coherent structures. Maximum foam extents were observed at 154m, indicating surface material moving substantially offshore relative to the small surf zone.

THIS PAGE INTENTIONALLY LEFT BLANK

TABLE OF CONTENTS

THIS PAGE INTENTIONALLY LEFT BLANK

LIST OF FIGURES

THIS PAGE INTENTIONALLY LEFT BLANK

LIST OF ACRONYMS AND ABBREVIATIONS

2D	2 dimensional
3D	3 dimensional
FAA	Federal Aviation Administration
FPS	frames per second
GCP	ground control point
HMS	Hopkins Marine Station
LCSs	Lagrangian coherent structures
MBNMS	Monterey Bay National Marine Sanctuary
P3S	Phantom 3 Standard
PIV	particle image velocimetry
VGCP	virtual ground control point
VLF	very low frequency
UAV	unmanned aerial vehicle

THIS PAGE INTENTIONALLY LEFT BLANK

ACKNOWLEDGMENTS

I would like to thank my advisor, Jamie MacMahan, for his guidance, intellect and patience to make this thesis happen. His passion for this area of study made the process fun and interesting (most of the time!). My sincerest gratitude to Casey Gon for helping me throughout the whole process and especially the encouragements when times were overwhelming. I want to thank my classmates for all of the help along the way. And most importantly I want to thank my wife, Kaley, for her patience throughout my time here at NPS. Her constant love, support, and willingness to pick up the slack when I was both physically and mentally absent made my time here easier.

THIS PAGE INTENTIONALLY LEFT BLANK

I. INTRODUCTION

Rocky shorelines are complex landscapes ranging from steep cliffs to terraces to sloping rock outcrops inundated with networks of channels and crevices. They are estimated to make up 75 percent of the world's coastlines (Davis and Fitzgerald 2004). Frequently exposed to high wave energy, the air and sun, and varying tides, rocky shorelines are often characterized as harsh and hostile environments (Davis and Fitzgerald 2004). Although harsh, rocky intertidal zones are home to an abundance of various plants, animals, and microorganisms. Rocky coasts are described as having rocky substratum mostly characterized as plunging cliffs or shore platforms (Trenhaile 2002). The latter is divided into two categories, Type A platforms and Type B platforms. Type A platforms are described as having a constant slope and Type B platforms are described as a relatively horizontal surface with an abrupt drop at the seaward edge (Sunamura 2015). As an important source of sediment for beaches and estuaries (Trenhaile 2002), there has been extensive research focusing on morphology and wave relationships in connection to erosional mechanisms and temporal scales (Trenhaile 2002; Stephenson and Thornton 2005; Beetham and Kench 2011; Marshall and Stephenson 2011; Sunamura 2015; Kennedy et al. 2017). Rocky shorelines can also be similar to rocky reef systems which are described as having variable cross-shore and alongshore bathymetry and irregular topography that can be either submerged or exposed depending on the tidal stage (Winter et al. 2017). Despite the prevalence of these coasts, there has been a sparse amount of research studying hydrodynamics on rocky shores (Davidson-Arnott 2010) with the exception of a recent study by Winter et al. (2017) on the hydrodynamics on a rocky reef-fringed coast. O'Donnell and Denny (2008) have measured hydrodynamic forces on a wave-swept rocky shore, but in relation to ecological habitats on the spatial scale of centimeters. They found that water breaking water velocities directly on the rocks can routinely reach a maximum of 10 m/s and reach up to 25 m/s during energetic storm events.

The goal of this study is optical imagery of wave-swept, surge-channel rip currents that are a persistent process that develops along rocky shorelines. To date, no observations have focused on these type of rip currents. Therefore, an initial discussion will focus on rip

currents that develop along sandy beaches that have been studied over the years. Rip currents are fast moving offshore flows of water responsible for transporting floating material such as bubbles, foam, sediment, organisms, and pollutants from the surf zone to the inner shelf (Shepard et al. 1941; Inman and Brush, 1973; MacMahan et al. 2006; Brown et al. 2009; Dalrymple et al. 2011). Bathymetrically-controlled rip currents are generated by alongshore variations in bathymetry leading to variations in alongshore wave breaking causing alongshore pressure gradients induced by wave set-up and set-down (Bowen 1969; Haller et al. 2002). Alongshore currents flow from higher to lower water levels where they converge into the offshore flow of the rip current (Bowen 1969; Dalrymple 1978; MacMahan et al. 2009). Wave climate, bathymetry, and tidal elevations determine the size and strength of rip currents (Dalrymple et al. 2011). Shepard et al. (1941) noted that the intensity of rip currents increases with increasing wave energy. The intensity of rip current flow is modulated at the infragravity band (0.004-0.04Hz) (Shepard et al. 1941; Shepard and Inman 1950; Sonu 1972; MacMahan et al. 2004a) as well as very low frequency motions (< 0.04Hz) (MacMahan et al. 2004b). MacMahan et al. (2006) partition the flow velocity into contributions from the mean rip velocity, infragravity pulsations, very low frequency pulsations (VLFs), and the tidal modulation. Mean rip current velocity was around 0.3 m/s, whereas rip current pulsations increased the flow velocity to 1 m/s. In addition, rip currents are modulated by tides, where decreases in the tidal elevation will inversely increase the rip current flow (Sonu 1972; Aagaard et al. 1997; Brander 1999; Brander and Short 2001; MacMahan et al. 2006; Dalrymple et al. 2011).

Studies on material transport (Smith and Largier 1995; Reniers et al. 2010; Brown et al. 2015; Kumar and Feddersen 2017) highlight the ability of rip currents as a transport mechanism; however, the dynamic signature of rip current circulations, driven by changes in wave conditions, VLF pulsations (4–30 min), infragravity pulsations (25–250 s), tidal modulations, and incident swell, make it difficult to determine when material within the surf zone will be transported offshore (Reniers et al. 2010). Brown et al. (2015) and Reniers et al. (2010) note the importance of VLFs, cross-shore oscillations at frequencies < 0.004 Hz (MacMahan et al. 2004b; Dalrymple et al. 2011), as the dominant exchange mechanism between the surf zone and inner shelf. Surface drifters deployed by Brown et al. (2015) as

part of a field experiment on a rip-channeled beach displayed two circulation patterns. The first as cross-shore exchange contained locally within the surf zone as drifters moved seaward from the shoreline and returned shoreward a small distance from where they started. The second pattern extended past the surf zone, moving farther alongshore and gradually back shoreward (Brown et al. 2015). Brown et al. (2015) found the extent of the drifters was typically one to two surf zone widths beyond the surf zone. Reniers et al. (2010) used Lagrangian coherent structures (LCSs) to identify the ejection of surf zone material. Similarly seen by Smith and Largier (1995), eddies form at the head of the rip current and can detach as the neck of the rip current dissipates, sending surf zone material offshore. Brown et al. (2015) and Kumar and Feddersen (2017) identify transient rip currents as mechanisms for exchanging material from the surf zone to the inner shelf. Kumar and Feddersen (2017) ran a coupled wave resolving and ocean circulation and wave propagation model and found that if a transient rip current was present, exchange velocity at three surf zone widths were 2–10 times larger than if a transient rip current was not present.

Breaking waves carry trapped air below the sea surface creating bubbles (Thorpe et al. 1999). As they reemerge on the surface they either pop or remain floating and coalesce with other floating bubbles forming patches of foam that can persist for 10–20 seconds (Thorpe et al. 1999). Rising bubbles can also feed on dissolved organic matter that may be in the water column (Velimirov 1980). The combination of bubbles and organic matter create sea foam. Heavy foam formation has been observed in the vicinity of kelp beds (Field et al. 1977; Velimirov et al. 1977). Velimirov (1980) found that kelp produces a mucilage, more so when waves would churn the kelp into neighboring rocks and damage them. The mucilage was an active agent in foam formation and additionally works to improve the stability of the foam (Velimirov 1980). Holland et al. (2001), Chickadel et al., (2003), and Holman and Haller (2013) all note the advantage of using bubbles and foam as passive tracers in optical imagery velocity calculation techniques.

Optical imagery of the nearshore offers a low-cost alternative to in situ sensors used in characterizing nearshore processes and alleviates some of the difficulties associated with these sensors such as biofouling, sensor deterioration, or flow disturbances (Holland et al.

1997). Measurements of nearshore fluid processes, foreshore topography, variable morphology, and wave climate can be quantified over a wide range of spatial (cm to km) and temporal (sec to yrs) scales (Holland et al. 1997). Images can be projected from 2-dimensional (2D) image coordinates into 3-dimensional (3D) world coordinates to a high degree of accuracy enabling the quantification of nearshore processes. Holland et al. (1997) tested the accuracy of using a calibrated camera system for field measurements comparing calibrated camera images to surveyed ground control points (GCPs). Holland et al. (1997) found the calibration results had an object space error that was small relative to the target and the accuracy was approximately equal to the survey accuracy of 1 cm. Optical sensors can be secured at fixed locations or fixed to aerial vehicles, both with tradeoffs in dwell and footprint (Holman and Haller 2013). Cameras at fixed locations offer unlimited dwell and the need to only resolve image geometry once but may tradeoff with its vantage point, some areas may not allow for a high enough vantage point resulting in a resolution degradation of sampling processes as the tilt of the camera becomes more horizontal (Holman and Haller 2013). Fixing cameras to aerial platforms offers higher vantage points and easier access to locations, however the movement of the platform requires constant image geometry calculations and a reduction in dwell time. Technological advances have led to the proliferation of large to small unmanned aerial vehicles (UAVs), in particular hobby sized quadcopters. These are becoming ideal platforms for collection as they are easy to fly and affordable.

A wide array of nearshore optical signatures can be exploited. Nearshore processes worldwide have been measured extensively with the Coastal Imaging Lab's Argus camera station. More recently, Holman et al. (2017) have used the Argus station processes with a small UAV quadcopter. These methods have been used to look at changing bar morphodynamics, wave run-up, and swash zone velocities to name a few. Wave and current dynamics are easily captured through observations of wave breaking, and variations in the reflection coefficient of water and the steep front face of waves allow for period, wavelength and direction of waves to be seen (Holman and Stanley 2007). Holman et al. (2017) explains that the reflection coefficient combined with the skydome radiance (brightness of the sky above) equal the intensity radiance captured by a camera. Time

exposures, a series of images averaged over time, use the brighter intensities to image areas of breaking waves which are indicative of sand bars. These can be used to track migrating sand bars over time. Longshore current estimations track smaller patches of foam (bright intensities) by collecting time series data from image pixels in longshore arrays (Chickadel et al. 2003; Holman et al. 2017). Particle image velocimetry (PIV) methods track features over time, such as foam, to quantify horizontal flow structures (Holland et al. 2001).

The goal of this thesis is to study a wave swept surge channel rip current on a rocky shoreline. Aerial imagery of the rocky shore surf zone at Stanford's Hopkins Marine Station is analyzed to characterize the surface flow of wave swept surge channel rip currents. Persistent bubbles and foam from breaking waves on surrounding rocks are used as passive tracers to describe the surf zone location, extent of the rip currents and cross shore transport, and the mean cross shore velocity of the rip current. These observations will serve to begin to capture a currently sparse information base on some of the rocky shoreline surf zone flow kinematics.

THIS PAGE INTENTIONALLY LEFT BLANK

II. METHODS

A. UAV PLATFORM

Aerial imagery of the rocky shoreline was obtained with a DJI Phantom 3 Standard (P3S) quadcopter (Figure 1). The P3S is a low-cost, easy-to-use commercial off-the-shelf system that is quoted to station keep at a vertical accuracy of + 0.5 meters and a horizontal accuracy of + 1.5 meters. It has a flight duration of approximately 25 minutes. The P3S includes a digital camera that is mounted to a 3-axis gimbal that provides a steady platform and 120° in tilting range. The digital camera has a 1/2.3-inch complementary metal-oxide semiconductor (CMOS) sensor allowing for stationary images to be resolved with 4000 x 3000 pixels (12.3 megapixels) and 30 frames per second (fps) video imagery to be resolved to 2.7k resolution (DJI 2018).

Figure 1. Image of the DJI Phantom 3 Standard. Digital camera with 3D gimbal shown below the UAS.

B. PHOTOGRAMMETRY

Images collected here are georectified to a world coordinate system following methods by Holman et al. (2017). Georectification from a moving platform requires that the image frame geometry for each image to be estimated (Holman et al. 2017). To solve for the image geometry, properties specific to the camera in use and information about the camera position and orientation relative to the reference coordinate system must be known (Holland 1997).

The camera specific properties are the intrinsic parameters describing the characteristics of the camera, lens, and image acquisition hardware (Holland 1997). These characteristics are the focal lengths in the U and V directions, the U and V coordinates of the geometric image center (or principle point) and the distortion coefficients (Holman et al. 2017). The intrinsic parameters allow for the correction of any lens distortion and transform the camera coordinates into geographic coordinates (Holman et al. 2017). There are multiple image processing toolboxes that are available for determining the intrinsic parameters. Here, the MATLAB camera calibrator application was used. Using the P3S drone camera, multiple photographs of a checkerboard at different angles were obtained and uploaded into the camera calibrator application. An output of the application are the intrinsic parameters of the P3S camera.

The geometric description of the camera position and the orientation relative to the reference (world) coordinate system are the extrinsic parameters (Holland 1997). The extrinsic parameters describe the camera x, y, and z location and include the camera's three viewing angles of azimuth, tilt, and roll (Holman et al. 2017). If the extrinsic parameters are known, they can be combined with the previously solved for intrinsic parameters to perform a projective transformation and the image coordinates can be mapped to geographic coordinates (Holman et al. 2017).

There are 11 unknowns that need to be solved for to georectify an image (Holman et al. 2017). The camera calibration used to calculate the intrinsic parameters account for 5 of these unknowns, the remaining 6 are the extrinsic parameters. If any of the extrinsic parameters are not known, they can be supplemented with ground control points (GCPs),

which are objects within the image field of view that have known locations. A single GCP can account for 2 unknown extrinsic parameters, because it contributes two values, a U and V coordinate (Holman et al. 2017). If no known extrinsic parameters exist, then a minimum of 3 GCPs would be required to georectify an image. Holman et al. (2017) tested the number of knowns and the number of GCPs and determined that positional accuracy of ground distance increased with an increased number of GCPs. Even with if specific extrinsic parameters known (x, y, z, and roll), requiring only 1 GCP, the ground distance accuracy was more accurate if there were no known extrinsic parameters and 4 GCPs (Holman et al. 2017). Based on the importance of GCPs, a minimum of 4 GCPs were used for georectification of aerial imagery collected for this effort.

C. FIELD METHODS

Aerial video imagery of the surf zone processes was collected along the rocky shoreline at Stanford's Hopkins Marine Station (HMS) in Pacific Grove, CA. HMS is a headland oriented approximately north/northwest on the southern coast of Monterey Bay. It is characterized by an irregular shoreline dominated by outcrops of rocks. The slope up to the headland is steep with highly variable bathymetry owing to the rocky shoreline. The shoreline is often surrounded by kelp beds.

In order to fly a drone at HMS, certain regulations had to be followed. The Federal Aviation Administration (FAA) requires all drones to be kept under 121 meters and if within 5 miles of an airport the control tower must be notified with contact information, location, duration, and height of the drone flight. The Monterey Airport is within this threshold and was notified before each flight. Because the area is near a flight path, drone flights were advised to be kept at a height under 60 meters. Monterey Bay is a national marine sanctuary (MBNMS) and also has rules regarding drone flights over the sanctuary. A permit must be obtained if wanting to fly over the sanctuary which starts at the mean high tide line. To keep within FAA and MBNMS regulations, an altitude of 60 meters and a position over land was chosen for the flights

Two rocky shoreline surge channels were chosen to study the rip current processes. These channels were the most prominent and persistent features (see Figure 2). The rip

channel to the north of the headland (Rip 1) is oriented at approximately 345°. The rip channel approximately shore normal to the headland (Rip 2) is oriented at 325°. A total of 27 flights were conducted on 7 different days over a 4-month period from January to April 2018 to observe the rip current flow in these two channels. Each recorded flight lasted approximately 14 minutes to keep data size manageable. Imagery was captured during varying tidal and wave conditions. Wave heights, direction, and period were obtained by the National Data Buoy Center (NDBC) buoy 46240, located approximately 0.5 km off of HMS in 17.8 m of water. Significant wave heights varied during the imagery collection time frame with lowest wave heights observed at 0.9 m and the highest waves observed at 1.82 m. Wave direction was predominantly from north/northwest and the wave period ranged from 9 to 13 s. Tidal elevations were measured at the NOAA tidal station 9413450 located on a pier approximately 2 km to the southeast of HMS. Wind speed and direction are also available at this tidal station. Wind speeds ranged from 0.9 m/s to 6.8 m/s with directions predominantly coming from the west/northwest.

The drone would station-keep at relatively the same location. Therefore, common fixed GCPs in the field of view were surveyed to avoid re-deploying and surveying GCPs for each effort. This allowed for rapid deployment of the drone with a single user for collection under various wave conditions at different tidal elevations. GCPs consisted of water towers, rocks, a concrete platform, and a solar panel system (Figure 2). The center of 9 GCPs were surveyed with the Ashtech ProMark 500 Real Time Kinematic (RTK) Global Positioning System (GPS) that provides centimeter accuracy after post-processing.

Figure 2. Image of Hopkins Marine Station. Red circles indicate locations of the nine fixed ground control points and green circles are locations of the two rip channels of interest.

D. DATA PROCESSING

The P3S is capable of obtaining high-resolution still imagery at an interval of 1 frame per 5 seconds. This sample frequency was not sufficient to resolve the sea and swell without aliasing. Because the channels are persistent features and do not change, a frequency of 2 Hz was sufficient to track particles such as bubbles and foam. The video setting on the P3S records 30 fps and was chosen for collection. Video from each flight was downloaded and decimated, splitting the video into still images, at a frequency of 2 Hz. For each flight this produced roughly 1600 distorted raw images (Figure 3a). A suite of open-source georectification Matlab programs is managed and updated by members of the Coastal Imaging Research Network on the website GitHub for UAV imagery. The surveyed GPS data were downloaded, processed and rotated to a local coordinate system such that the HMS headland is described into a cross- and alongshore orientation.

To run the UAV toolbox and georectify the images, GCPs were identified in an input file and then selected within the first image frame. Since the drone is not fixed to a position and is subject to small drifts, the direction of the camera shifts is accounted for in each frame. This requires that the geometry for each frame has to be solved. Holman et al. (2017) toolbox utilizes an automated feature to recognize objects referred to as "virtual" GCPs (VGCPs), which differ from the GCPs. In this case, white boards were placed in the darker vegetation area throughout the area of interest. The contrast of the bright boards against the dark vegetation provides an ideal colormap for image pixel recognition algorithms to find and for estimating the white boards center of mass based on pixel intensity. The VGCPs are a more efficient method of estimating the frame geometry for each image. The georectification provides a true position of the physical processes and their evolution that can now be quantified (Figure 3b).

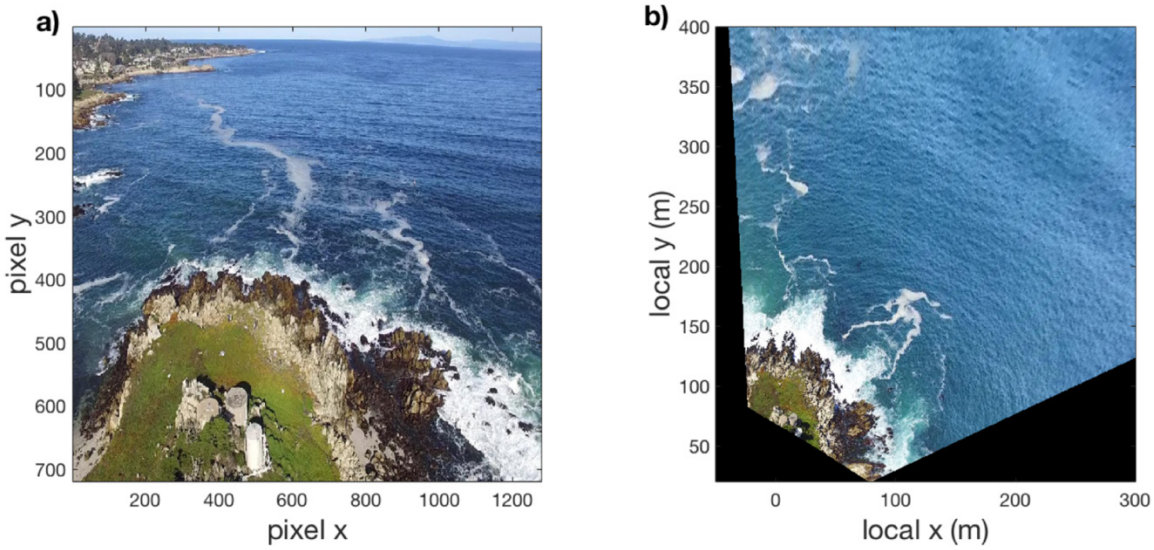

Figure 3. Image of Hopkins Marine Station. (a) Raw pixel image; (b) georectified, georeferenced and rotated image.

The series of images collected for the flight were averaged together to create a time exposure image (Holland 1997) (Figure 4a). The image is composed of individual pixels, small square picture elements. Each pixel has an associated color or gray intensity (brightness) level ranging from 0 to 256, which range from dark to light (Friel 2000). Using the time exposure image, the red green blue (RGB) color intensities for the image pixels were used to create contours of the bubble zone and rip current extents. Figure 4b shows a distinct difference in color intensity due to breaking waves and resulting bubble and foam fields. This is where the intensity thresholds were determined to create the bubble zone contours. For most flights, a threshold value of 150 was chosen as a good representation of the bubble zone contour. Once a threshold was identified and contoured, the intersection of pixel arrays (Figure 4a) and contour lines was calculated for each flight and determined to be the extent for that flight.

The offshore extent of material that was transported by rip currents was evaluated by foam that was ejected from the bubble zone via a rip current. The foam extent color intensity was not as apparent so the variance of the dark and bright images was used to find an intensity threshold. A variance threshold around 2500 was used to plot the foam extent contours (Figure 4c). This process was repeated for each flight to determine where the extents of the bubble zone and rip current (Figure 4d blue line), and foam (Figure 4d red line) for each day existed.

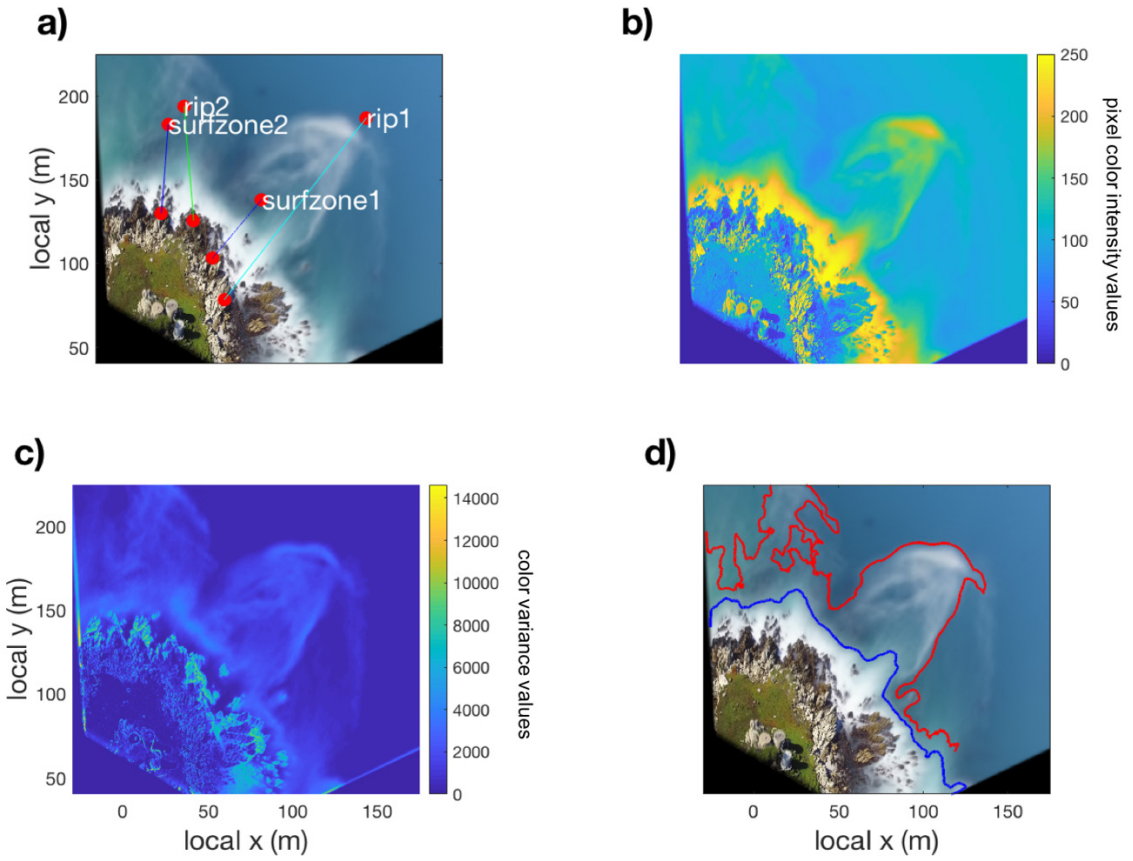

Figure 4. Image Process for Surf Zone and Foam Extent. (a) Time average rectified image with pixel array lines of rip1, rip2, surf zone1, and surf zone 2 (b) rectified image displayed by pixel color intensity (c) rectified image displayed by color variance (d) rectified image with contour of bubble zone and rip current extent in blue and contour of extent of foam in red.

One of the goals for this project was to determine rip current velocity from aerial imagery. The bubble region created at the shoreward onset of the rip channel was used as a tracer to measure velocity as the foam ejected beyond the surf zone. A few methods were attempted to calculate the velocity based on these foam tracers. Automating code for foam trajectory patterns as function of time was proven difficult across the entire pathway. In particular, as the foam moved farther offshore, the calculated velocities were noisy and unrealistic. A few cases resulted in velocities increasing and others resulted in large positive and negative velocities occurring within short distances. Open-source particle image velocimetry (PIV), which tracks features over time resulting in the associated flow

velocity components (Holland 2001), was applied to these images. The PIV method failed owing to the complexity of the shoreline, the presence of waves and corresponding shadows, non-stationarity of the flows, and coarse resolution. Therefore, a manual method was found to provide the most consistent estimates of velocities.

Cross-shore pixel arrays were determined such that the line was centered in each channel of interest. The pixel intensity was calculated along those lines for the series of images. The pixel array (Figure 5a) highlights the cross-shore movement of foam as a function of time. A low-pass filter was applied to the pixel array to filter out the influence of the sea and swell waves (Figure 5b). The slope of the ridge of the pixel intensity as a function of cross-shore distance and time represents an individual foam-streak velocity. The individual foam streak velocities were averaged over deployments and represent the mean surface rip current velocity for a rocky channel.

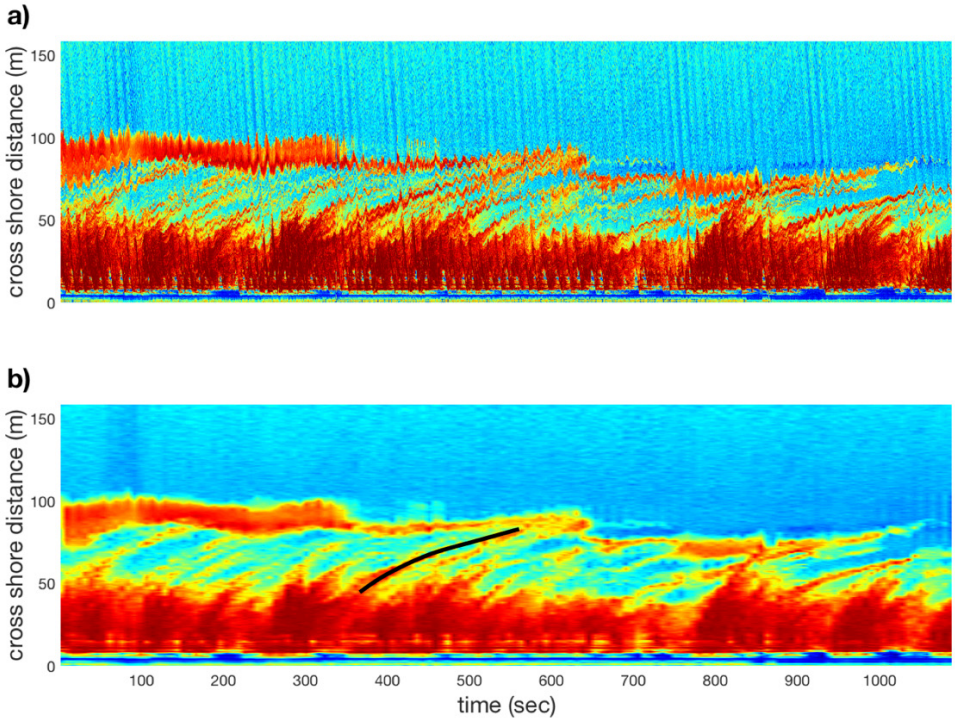

Figure 5. Pixel Color Intensity Array Used for Velocity Determination. (a) Unfiltered cross shore pixel array (b) filtered every 15 seconds, foam ejection paths traced (black line) to calculate slope.

THIS PAGE INTENTIONALLY LEFT BLANK

III. RESULTS

A. BUBBLE ZONE EXTENT

Time exposure images of each day show that the shoreline at HMS is surrounded by a bubble zone rather than a surf zone (Figure 4d blue line). The extent of bubble zones 1 and 2 ranged between 8.4–22.8 m, and 5.6–21.9 m (Figure 6). The respective mean offshore extents were 13.6 m and 14.1 m. Scatter points of wave height vs cross-shore distance indicated that the extent of the bubble zone increases with increasing wave heights (Figure 6). The extent of the bubble zone is further modulated by tidal elevations, as the tidal elevation decreases the extent of the bubble zone will increase (Figure 6).

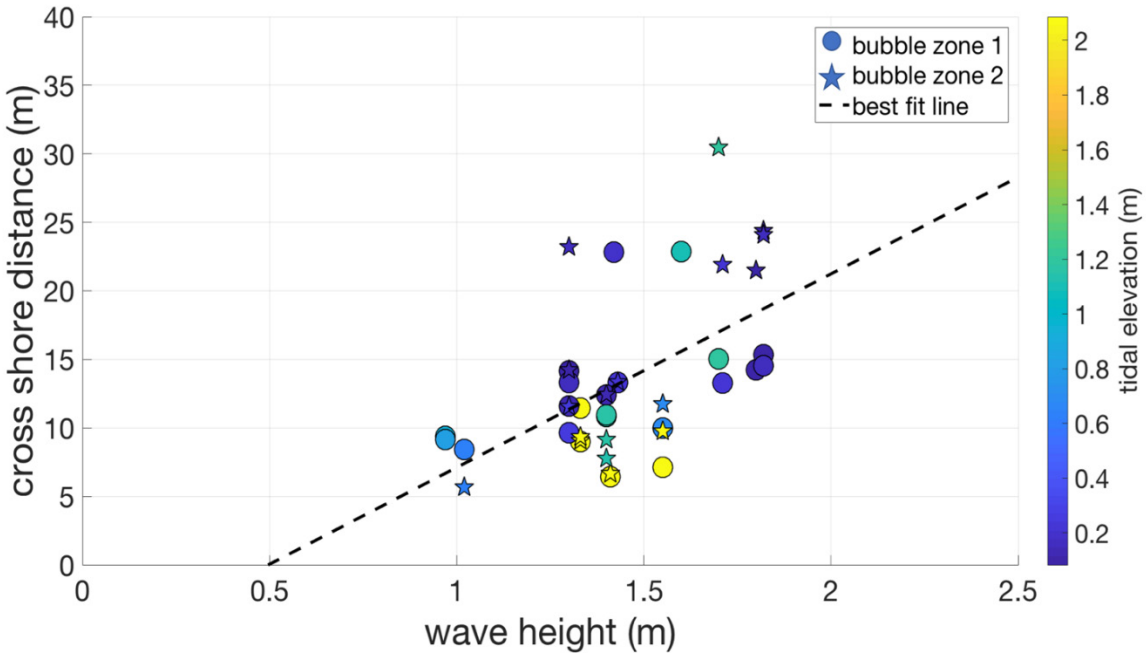

Figure 6. Scatter Plot of Bubble Zone Cross-Shore Distance. The x axis is significant wave height (m), the y axis is the cross-shore distance (m), the colorbar is tidal elevation (m). Circle markers indicate values for bubble zone 1 and stars indicate values for bubble zone 2.

B. RIP CURRENT EXTENT

Similar to plumes of sediment in the rip current head of sandy shore rip currents, the rocky shore rip current has a plume of bubbles that extend farther than the bubbles generated along the rocks outside the rip channel, indicating the extent of the rip current. To unbias the distance due to the longer inshore channel, the rip current pixel arrays were normalized to what was determined to be the shoreline of the rocky shore on the bubble zone pixel array. The distance between the rocky shore shoreline and the rip channel shoreline were subtracted. The extent of the rip currents in channels 1 and 2 ranged between 14.3–49.2 m, and 8.8–33.1 m (Figure 7). The respective mean offshore extents were 33.1 m and 18.1 m. Like the bubble zone extent, as wave heights increase, the extent of the rip current increases (Figure 7) and inversely, as tidal elevations decrease rip current extents increase.

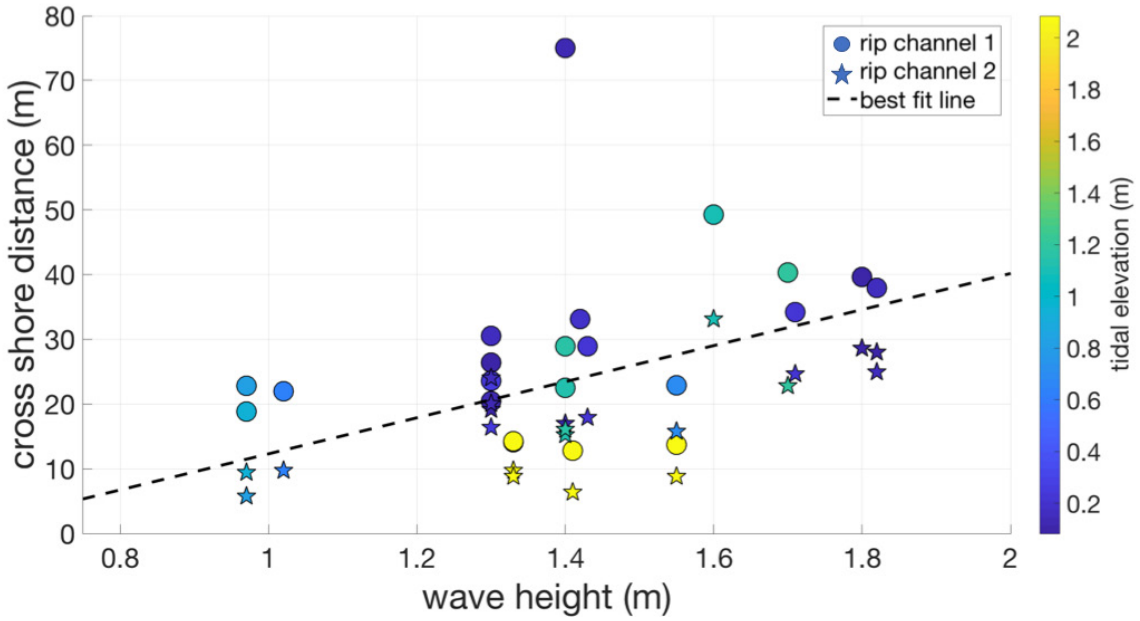

Figure 7. Scatter Plot of Rip Current Cross-Shore Distance. The x axis is significant wave height (m), the y axis is the cross-shore distance (m), the colorbar is tidal elevation (m). Circle markers indicate values for rip channel 1 and stars indicate values for rip channel 2.

C. FOAM EXTENT

The drone imagery was analyzed to determine when foam was ejected and the extent it travelled offshore in relation to the bubble zone (Figure 4d red line). The mean foam extent for rip channel 1 was 93.6 m offshore, the maximum extent was 153 m when significant wave height was 1.6 m (Figure 8). The minimum foam extent was 42 m offshore and occurred during the lowest significant wave height for the study. The mean foam extent for rip channel 2 was 69.3 m. The maximum extent was 154 m during higher significant wave heights. The minimum was 20 m during the lowest recorded significant wave height for the study. Persistent foam was generated four out of the seven days flights occurred. Foam generation appears to be dependent on wave heights. As wave height increases, foam generation increases and the extent of the foam is farther offshore (Figure 8).

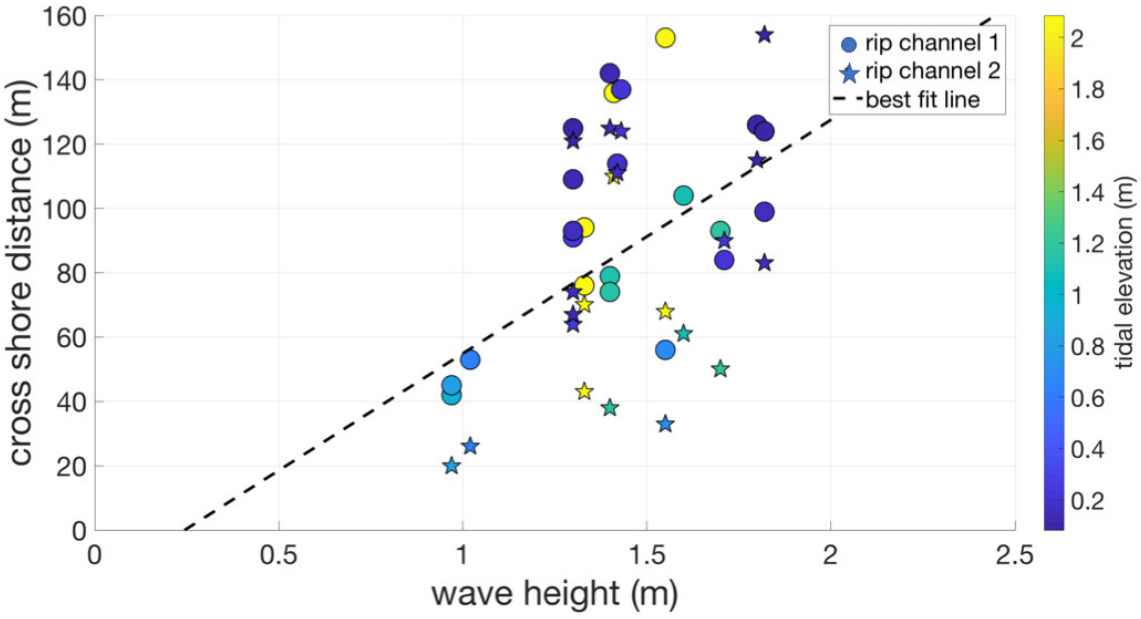

Figure 8. Scatter Plot of Foam Cross-Shore Distance. The x axis is significant wave height (m), the y axis is the cross-shore distance (m), the colorbar is tidal elevation (m). Circle markers indicate values for foam ejected from rip channel 1 and stars indicate values foam ejected from for rip channel 2.

D. MEAN CROSS-SHORE VELOCITY

The computed cross-shore velocities of each rip current pulse as a function of cross-shore distance, as determined from foam ejections in figure 5, are averaged over each day a flight was conducted. The resulting cross-shore velocities of the surface material transport associated with rip channels 1 and 2 are generated (Figure 9 and 10). The computed velocities did not contain the steady state rip current velocity. The density of bubbles made it difficult to identify the slope of the rip current in the plotted pixel arrays.

In rip channel 1, the mean velocities start just inside the bubble zone and are then tracked outside of the bubble zone (Figure 9). The first 90 m of velocity calculations were found to be not significant at the 95 percent confidence interval. The calculated velocities fit within a range of 0.15 m/s to 0.3 m/s. It is not until the last 20 m that the velocity calculations are significant at the 95 percent confidence interval. At the outer extent, the velocity decreases to less than 0.1 m/s indicating an abrupt stop in the flow. While the majority of the velocity calculations along the cross-shore pixel array is not significant, it is for the last 20 m indicating a decreasing trend in velocity as the flow travels offshore. Three of the seven averaged flights were statistically significant at the beginning and end points of the pixel array. The remaining four were not statistically significant throughout the whole pixel array. Confidence intervals for differing tidal elevation days and wave days overlapped making it difficult to compare cross-shore velocity under varying environmental conditions. The calculated velocities are linear meaning that the velocities for the rip channel are fairly constant which would explain the lack of velocity variation in from the foam slope calculations.

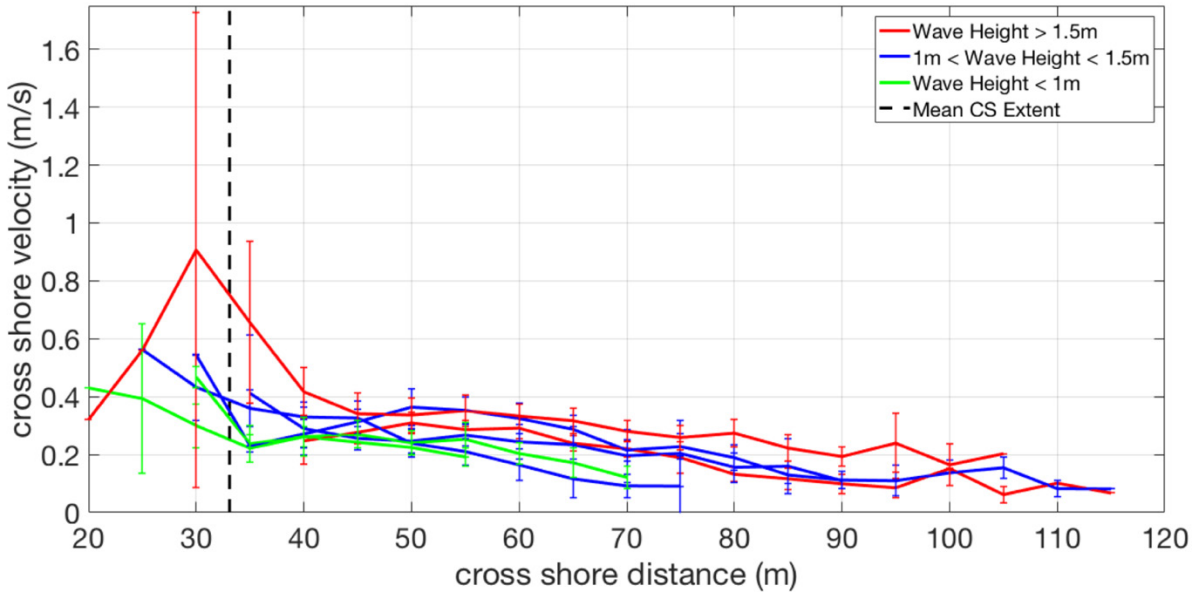

Figure 9. Mean Cross-Shore Velocities in Rip Channel 1. The x axis is cross-shore distance (m) and the y axis is mean cross-shore velocity (m/s). Lines are colored by wave height; red are wave heights above 1.5m, blue are wave heights between 1m – 1.5m, green are wave heights less than 1m, dashed line indicates the rip current mean cross-shore extent.

The same trend persisted for rip channel 2, with the exception of where the velocities were tracked in relation to the mean rip current extent. The velocity calculations begin just at or 5 to 10 m beyond the bubble zone (Figure 10). The velocity calculations are similar to those for rip channel 1. The first 2/3 of calculated velocities are not statistically significant at the 95 percent confidence interval. The last 1/3 does show statistical significance for four out of the seven days. For rip channel 2, the velocities range in between 0.2 m/s and 0.4 m/s and decrease to less than 0.1 m/s for the last 1/3 of the cross-shore distance. Like rip channel 1, the overall velocity trend is flow decreasing as it moves offshore. The slopes for each flight day are linear indicating that the cross-shore flow is constant.

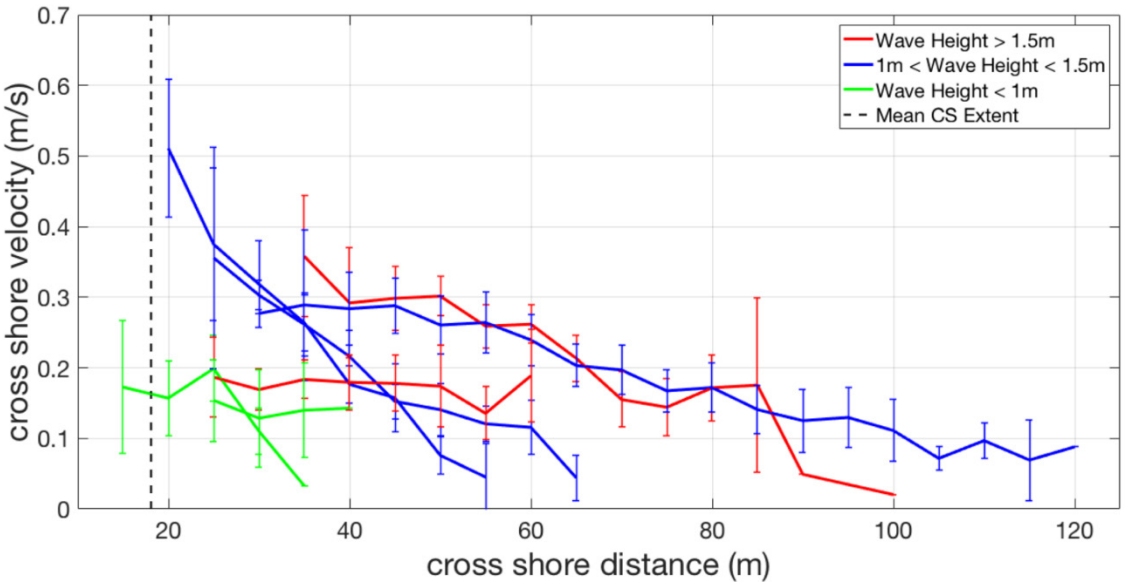

Figure 10. Mean Cross-Shore Velocities in Rip Channel 2. The x axis is cross-shore distance (m) and the y axis is mean cross-shore velocity (m/s). Lines are colored by wave height; red are wave heights above 1.5m, blue are wave heights between 1m and 1.5m, green are wave heights less than 1m, dashed line indicates the rip current mean cross-shore extent.

IV. DISCUSSION

A. HOPKINS MARINE STATION BATHYMETRY

Surface flow characteristics of rip channels on a rocky shoreline at Hopkins Marine Station show similarities and differences to rip currents found on sandy beaches. HMS's shoreline is vastly different than that of a sandy beach and does not quite fall into the Type A or Type B rock platforms described by Sunamura (2015). It does however, share morphologic similarities to a rocky reef system; irregular bathymetry consisting of rocks of varying size and location supporting networks of channels connected to a steep land boundary. At HMS, the networks of channels converge to primary channels directing flow offshore resulting in stationary rip currents. The geometry of these primary channels will influence the strength of the rip currents, allowing them to extend well beyond the turbulent bubble zone left by wave breaking on HMS's rough and irregular rocky bathymetry. Deny et al. (2003) investigated the amplification of wave induced flow resulting from rocky shore topography. Deny et al. (2003) show that the interaction of headland type topography and broken waves will create limbs that collide and may produce a localized jet. Video imagery of rip channel 1 show this interaction of broken waves, a collision of refracted waves initiates flow offshore (Figure 11). Rip channel 1 appears to be a combination of the topographical effect described by Deny et al. (2003) and a network of feeder channels that further feed the larger surge channel with offshore moving water.

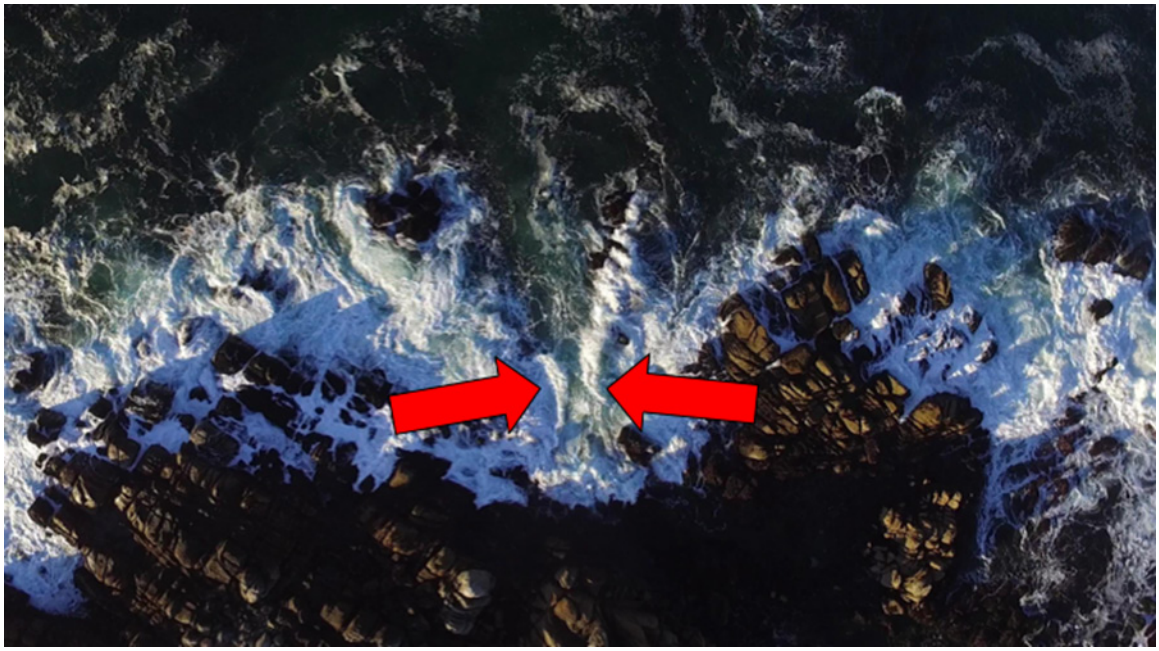

Figure 11. Image of Rip Channel 1. Red arrows point to the leading edges of refracted broken waves.

The irregular bathymetry plays an important role in steering the flow. Time exposure images for each day were analyzed to determine the effects the bathymetry may have. An outcrop of rocks to the northeast of rip channel 1(Figure 12 red circles) steers the flow at tidal elevations less than 2 m (Figure 12 red arrows). Tidal elevations above 2 m submerge these rocks and the flow travels in a northeasterly direction (Figure 12).

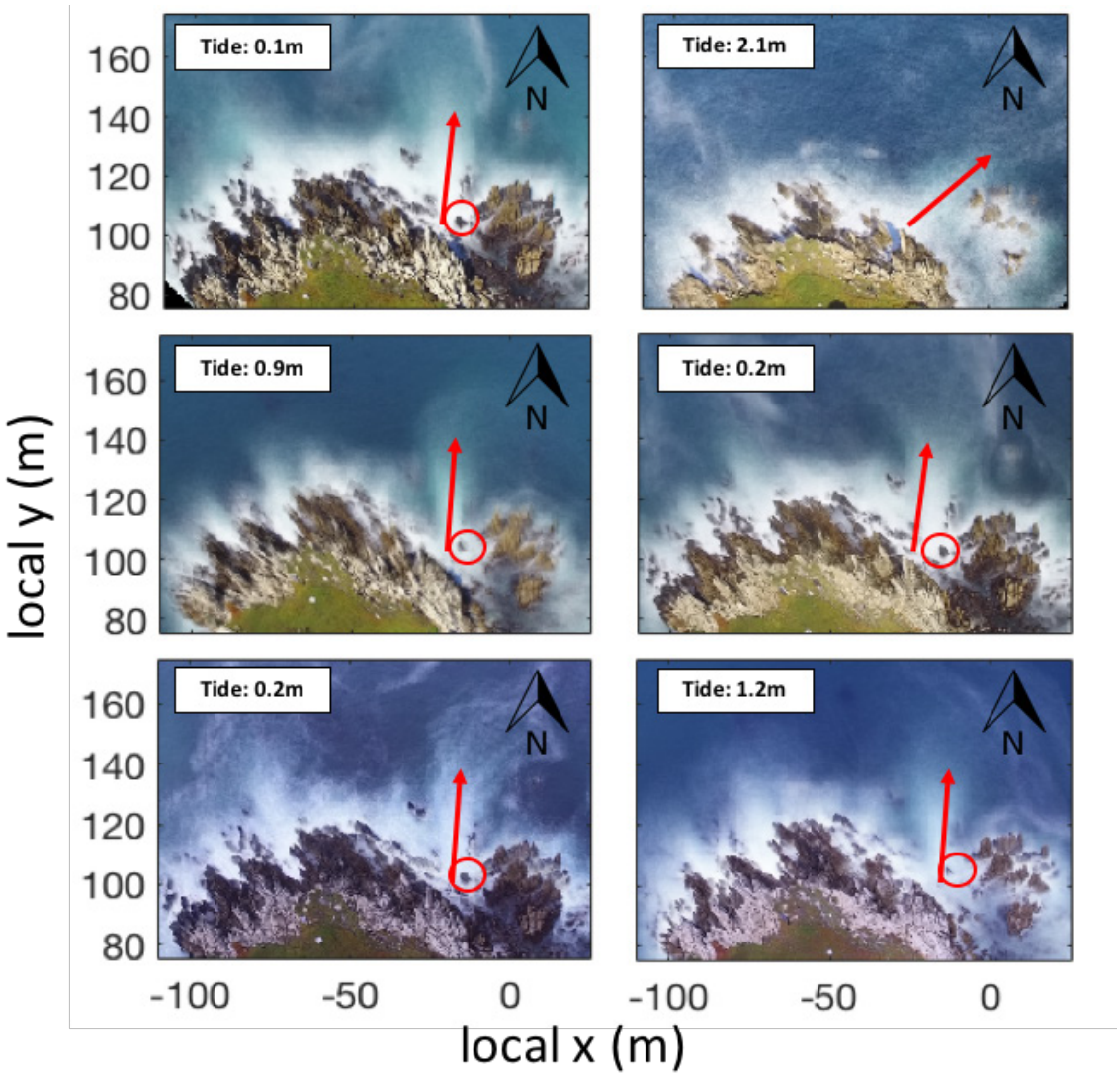

Figure 12. Time Exposure Images of Various Tidal Elevations. Red arrows indicate direction of surface and red circles highlight outcrop of rocks to the northeast of rip channel 1.

B. BREAKING WAVES

There are multiple types of rip currents that occur on sandy beaches, generally though, rip currents are a result of alongshore variations in bathymetry which create alongshore variations in wave breaking (MacMahan et al. 2006, Dalrymple et al. 2011). Waves carry energy, mass, and momentum expending energy as they break and dissipate across the surf zone. The differences in wave breaking induce differences in mean water levels, where the shoaling regions have a higher mean water level than the rip channel

region (Bowen 1969; Sonu 1972; Aagaard et al. 1997; Brander and Short 2001; MacMahan et. al. 2006; Dalrymple et al. 2011). The differences in mean water level create a pressure gradient where water will flow from higher to lower mean water levels. This sets up the basic circulation pattern of a rip current on a sandy beach. Waves break over the shoal and create alongshore feeder currents that converge into an offshore flowing rip current. This circulation pattern is not observed on the rocky shoreline at HMS. Video imagery show waves breaking as they encounter the various rock outcrops up to the shoreline. In the time exposure imagery, there is no indication of a breaker line usually associated with time exposure imagery on a sandy beach. Instead the time exposure images show an area inundated with bubbles depicted as a bright zone off the rocky shoreline up to the bubble zone contour (Figure 4d). As the waves break across the rocks, the offshore directed water surges back through the network of channels and in some areas, converge to a larger surge channel.

C. BUBBLE ZONE

On sandy beaches, wave breaking is the dominant hydrodynamic process as well as an important boundary as it delineates between the surf zone, the region extending from the seaward boundary of wave breaking to the shoreline, and the inner shelf which is seaward of the surf zone and shoreward of the mid-shelf (Dalrymple et al. 2011). HMS does not appear to have a traditional surf zone as the waves do not break until they reach the rocks. It does however, generate a dense area of bubbles owing to the waves breaking over the irregular bottom and the interaction with return channel flow (Figure 4d). Vagle et al. (2005) discusses bubble walls in the surf zone, defined as dense assemblages of bubbles generated by breaking waves which can persist for up to 30 minutes. The bubble zone around HMS is more representative of a bubble wall. Vagle et al. (2005) observed bubble wall spread, the difference between the most shoreward and seaward location, was between 10 m and 40 m in the absence of rip currents and that the spread increased to between 22 m and 60 m in the presence of rip currents. This is approximately a 50 percent increase in spread. A similar spread pattern is seen on the rocky shoreline at HMS. Outside the rip channels the bubble spread ranges between 13.6 m and 14.1 m. In the rip channels the spread increases to 33.0 m and 18.1 m for rip channels 1 and 2 respectively. The data

collected by Vagle et al. (2005) showed coherence with longer period variability in bubble plumes during large breaking events and rip current events. HMS shoreline creates persistent, stationary rip currents and video imagery analyzed for this study show the persistence of the bubble walls in the rip currents and an increase in bubble zone extents and foam generation during larger wave days (see figures 6,7,8).

It is possible that the farther extent of the bubble zone in the rip channels are a function of various bubble sizes. Measurements of bubble size were not gathered here, however, Vagle et al. (2005) described the average bubble size of the bubble wall in the presence of a rip current to be 100 μm and the average bubble size of the bubble wall in the absence of a rip current to be 40 μm. The bubble radius determines how quickly the bubble will rise, larger bubbles will rise faster than smaller bubbles. Enhanced turbulence levels in rip currents however, will suspend a significant proportion of larger bubbles in the water column driving the distance the bubble travels farther (Vagle et al. 2005). The water around the rocky shoreline is more turbulent owing to the irregular and rough bathymetry. As the tidal elevation decreases, more of the rocky bathymetry is exposed (Figure 12) and influences the creation of bubbles. Larger waves will also act to generate more bubbles. The 25 flights show that the extent of the bubble region corresponds to both wave height and tidal elevation (Figures 6,7,8). As the wave height increases the extent of the bubbles increases. This is further amplified with a decrease in tidal elevation.

D. CROSS-SHORE VELOCITY

Average cross-shore velocities have been measured to be between 0.3 m/s and 0.5 m/s (MacMahan et al. 2006; Dalrymple et al. 2011). Attempts were made to measure the steady state rip current velocity on the rocky shoreline at HMS. This proved to be problematic optically, as the area was inundated with bubbles making it difficult to determine any slope patterns in figure 5 for the steady state rip current. Foam left the dense bubble zones, seen as streaks in figure 5, and calculations of slope were made for offshore velocities of the rip currents. Vagle et al. (2005) noted that the steady surface flow of present rip currents would carry debris and foam offshore with a velocity around 0.1 m/s. Vagle et al. (2005) and Smith and Largier (1995) both observed rip currents from a pier at

Scripps in La Jolla, CA and noted that the narrow jets diffuse as they moved away from shore resulting in reduced flow the farther the flow extended. Measured cross-shore velocity on the rocky shoreline show similar results for measurements that were statistically significant at the beginning and ends of the image pixel arrays (Figures 9 and 10). Three out of the seven mean flights for rip channel 1 showed statistical significance at the end points and four out of seven mean flights showed statistical significance at the end points. While it is difficult to get specific calculations for the mean cross shore velocities along the pixel array due to the wide spread of mean cross-shore velocities, it can be assumed that there is a decrease in velocity as the flow travels offshore with faster velocities occurring near the extent of the bubble zones. Dependence on tidal elevation and wave heights could not be determined with certainty either, due to the overlapping confidence intervals for the majority of mean flights (Figures 9 and 10).

E. CROSS-SHORE TRANSPORT

Converging offshore foam streaks ejected from the rip channels are indicative of material exchange from the rocky shoreline. The foam streaks are LCSs, revealing where material such as organic material, sediment, humans, and mines will converge and travel. Reniers et al. (2010) highlighted the importance of LCSs as indicators of material exchange from the surf zone to the inner shelf. VLFs pulsate the rip current and will cause the LCSs to separate from the main rip current circulation transporting material offshore (Reniers et al. 2010). The period of foam ejections from the rocky shore rip channel indicate that a similar process may be occurring on the rocky shoreline. From figure 5, ejections of foam were marked. The time between each ejection was calculated and then averaged over the time series to get an average period for the foam ejections. The rip channel pulses ranged from 40 s to 62 s indicating that the foam ejections are a result of the waves.

Pixel array analysis show that on days of foam generation, the transport is offshore with no return. This is verified with a separate experiment where 100% of lagrangian drifters released from the shore of rip channel 1 immediately left the shoreline traveling along the foam lines (Figure 13). This differs from previous experiments of rip currents on sandy beaches. MacMahan et al. (2010) deployed a number of drifters and found that the

drifters exited the surf zone infrequently, 17% exited per hour. Brown et al. (2015) performed a similar experiment to observe cross-shore exchange between the surf zone and inner shelf. Drifters released displayed two patterns: 1) drifters moved seaward and returned shoreward quickly a short distance from where they were released indicating a locally contained cross-shore exchange system and 2) where drifters traveled farther both seaward and in the alongshore direction then gradually shoreward (Brown et al. 2015).

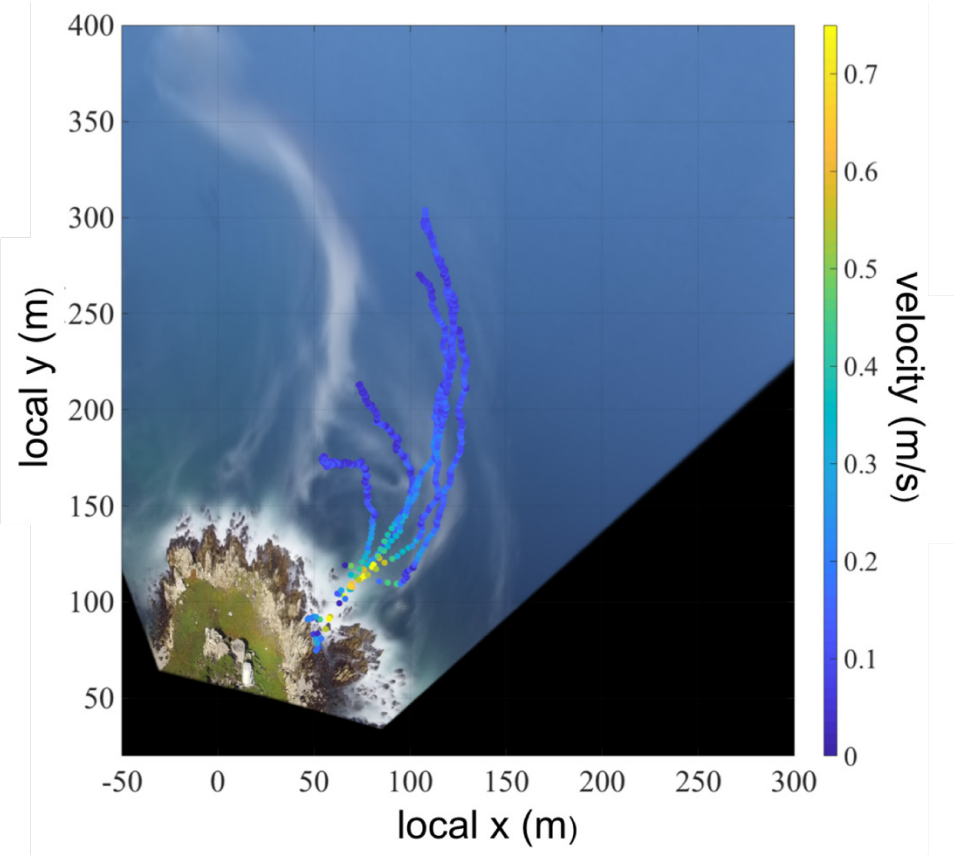

Figure 13. Time Exposure for UAV Flight on January 23, 2018. Circles are drifter positions colored by velocity.

THIS PAGE INTENTIONALLY LEFT BLANK

V. CONCLUSION

Optical imagery captured with a station keeping UAV was analyzed to investigate the surface flow of wave swept surge channel rip currents on a rocky shoreline in Pacific Grove, CA. A total of 25 flights were flown over seven different days from January 2018 to April 2018 during varying wave and tidal conditions. Georectified aerial imagery allowed for some surface flow characterization of rip currents on a rocky shoreline. A major difference is the lack of a surf zone at the rocky shoreline. Time exposure imagery on sandy beaches show concentrated bright features indicative of breaking waves influenced by meandering sand bars. Here, the waves break on the rocks and generate a dense bubble zone. The rocky shoreline bathymetry is significantly different than the smooth sandy shorelines. The bathymetry at HMS is irregular and rough and supports a network of channels. As water is transported onshore it rushes through the rocks and works its way offshore through the many channel systems. Some of these channels converge to a larger channel, resulting in the surge channel rip currents seen along the shoreline. These persistent, stationary rip currents carry material immediately offshore. A number of drifter deployments in the same rip channel studied here, had 100% of the drifters move immediately offshore. This is significantly different than cross-shore transport observed MacMahan et al. (2010) and Brown et al. (2015). Drifters exited the surf zone infrequently during these experiments. Similar to sandy beaches, wave heights and tidal elevation will modulate the observed features. The bubble zone extent, rip current extent, and the foam generation all saw an increase when significant wave heights were higher, farther extents were also observed during lower tidal elevations. Cross-shore velocities were difficult to measure with the optical approach conducted here due to the density of bubbles close to the rocky shoreline. Foam trajectories were able to be measured as they were ejected out of the bubble zone. The trajectories were linear, indicating a constant velocity and decaying as the flow moved offshore. Similar to sandy shoreline rip currents, the rip currents experienced a pulsation at wave group frequencies seen in the average period foam was ejected from the rip current. Rip currents on rocky shorelines share some commonality with sandy shore rip currents but also display vastly different flow patterns. Continued studies

of these stationary features are needed to fully understand the hydrodynamics processes occurring on the rocky shoreline.

LIST OF REFERENCES

Aagaard, T., B. Greenwood, and J. Nielsen, 1997: Mean currents and sediment transport in a rip channel. *Marine Geology,* **140**, 25–45, https://doi.org/10.1016/S0025-3227(97)00025-X.

Beetham, E. P., P. S. Kench, 2011: Field observations of infragravity waves and their behavior on rock shore platforms. *Earth Surf Process Landforms*, **36**, 1872–1888, https://doi:10.1002/esp.2208.

Bowen, A. J., 1969: Rip currents: Theoretical investigations. *J. Geophys. Res*., **74**, 5467–5478, https://doi:10.1029/JC074i023p05467.

Brander, R. W., 1999: Field observations on the morphodynamic evolution of a low-energy rip current system. *Marine Geology,* **157**, 199–217, https://doi.org/10.1016/S0025-3227(98)00152-2.

Brander, R. W., A. D. Short, 2000: Morphodynamics of a large-scale rip current system at Muriwai Beach, New Zealand. *Marine Geology*, **165**, 27–39, https://doi.org/10.1016/S0025-3227(00)00004-9.

Brander, R.W., A. D. Short, 2001: Flow kinematics of low-energy rip current systems. *J. Coast. Res.* **17**, 468-481.

Brown, J., J. MacMahan, A. Reniers, and E. Thornton, 2009: Surf zone diffusivity on a rip-channeled beach. *J. Geophys. Res.,* **114**, https://doi.org/10.1029/2008JC005158.

Brown, J. A., J. H. MacMahan, A. J. H. M. Reniers, and E. B. Thornton, 2015: Field observations of surf zone—Inner shelf exchange on a rip-channeled beach. *J.Phys.Oceanogr.,* **45**, 2339–2355, https://doi.org/10.1175/JPO-D-14-0118.1.

Chickadel, C. C., R. A. Holman, and M. H. Freilich, 2003: An optical technique for the measurement of longshore currents. *J.Geophys.Res.,* **108**, https://doi.org/10.1029/2003JC001774.

Dalrymple, R. A., 1978: Rip currents and Their Causes. *Proceedings of the Sixteenth Conference on Coastal Engineering*, 1414–1427, https://doi.otg/10.1061/9780872621909.085.

Dalrymple, R. A., J. H. MacMahan, A. J. H. M. Reniers, and V. Nelko, 2011: Rip Currents. *Annu. Rev. Fluid Mech.,* **43**, 551–581, https://doi.org/10.1146/annurev-fluid-122109-160733.

Davis, R. and Fitzgerald, D, 2004: *Beaches and Coasts.* Blackwell Science Ltd, 432 pp.

Denny, M. W., L. P. Miller, M. D. Stokes, L. J. H. Hunt, and B. S. T. Helmuth, 2003: Extreme water velocities: Topographical amplification of wave-induced flow in the surf zone of rocky shores. *Limnol. Oceanogr.,* **41**, 1-8.

DJI, 2018: Phantom 3 Standard Specs. Assessed 02 September 2018, https://www.dji.com/phantom-3-standard/info.

Friel, J., Grande, J., and D. Hetzner, 2000: *Practical guide to image analysis.* ASM International, 290 pp.

Haller, M. C., R. A. Dalrymple, and I. A. Svendsen, 2002: Experimental study of nearshore dynamics on a barred beach with rip channels. *J. Geophys. Res.,* **107**, 1-21, https://doi.org/10.1029/2001JC000955.

Holland, K. T., J. A. Puleo, and T. N. Kooney, 2001: Quantification of swash flows using video-based particle image velocimetry. *Coastal Engineering,* **44**, 65–77, https://doi.org/10.1016/S0378-3839(01)00022-9.

Holland, K., Holman, R., Lippmann, T., Stanley, J., and Plant, N., 1997: Practical use of video imagery in nearshore oceanographic field studies. *Oceanic Engineering, IEEE Journal of,* **22**, 81–92.

Holman, R. A., J. Stanley, 2007: The history and technical capabilities of Argus. *Coastal Engineering,* **54**, 477–491, https://doi.org/10.1016/j.coastaleng.2007.01.003.

Holman, R., Brodie, K., and Spore, N., 2017: Surf Zone Characterization Using a Small Quadcopter: Technical Issues and Procedures. *Geoscience and Remote Sensing, IEEE Transactions On,* **55**, 2017–2027.

Holman, R., M. C. Haller, 2013: Remote Sensing of the Nearshore. *Annu. Rev. Mar. Sci.,* **5**, 95–113, https://doi.org/10.1146/annurev-marine-121211-172408.

Inman, D. L., B. M. Brush, 1973: The Coastal Challenge. *Science,* **181**, 20–32.

Kennedy, D. M., M. A. Coombes, and D. N. Mottershead, 2017: The temporal and spatial scales of rocky coast geomorphology: A commentary. *Earth Surf. Process. Landforms,* **42**, 1597–1600, https://doi.org/10.1002/esp.4150.

Kumar, N. and F. Feddersen, 2017: The effect of stokes drift and transient rip currents on the inner shelf. part I: No stratification. J. Phys. Oceanogr., **47**, 227–241, https://doi.org/10.1175/JPO-D-16-0076.1.

MacMahan, J. H., A. J. H. M. Reniers, E. B. Thornton, and T. P. Stanton, 2004a: Surf zone eddies coupled with rip current morphology. *J. Geophys. Res.,* **109**, https://doi.org/10.1029/2003JC002083.

MacMahan, J. H., A. J. H. M. Reniers, E. B. Thornton, and T. P. Stanton, 2004b: Infragravity rip current pulsations. *J. Geophys. Res.,* **109**, https://doi.org/10.1029/2003JC002068.

MacMahan, J. H., E. B. Thornton, and A. J. H. M. Reniers, 2006: Rip current review. *Coastal Engineering,* **53**, 191–208, https://doi.org/10.1016/j.coastaleng.2005.10.009.

MacMahan, J., J. Brown, E. Thornton, A. Reniers, T. Stanton, M. Henriquez, E. Gallagher, J. Morrison, M. J. Austin, T. M. Scott, and N. Senechal, 2010: Mean Lagrangian flow behavior on an open coast rip-channeled beach: A new perspective. *Marine Geology,* **268**, 1–15, https://doi.org/10.1016/j.margeo.2009.09.011.

Marshall, R. J. E., W. J. Stephenson, 2011: The morphodynamics of shore platforms in a micro-tidal setting: Interactions between waves and morphology. *Marine Geology,* **288**, 18–31, https://doi.org/10.1016/j.margeo.2011.06.007.

Naylor, L. A., W. J. Stephenson, and A. S. Trenhaile, 2010: Rock coast geomorphology: Recent advances and future research directions. *Geomorphology,* **114**, 3–11, https://doi.org/10.1016/j.geomorph.2009.02.004.

O'Donnell, M. J., M. W. Denny, 2008: Hydrodynamic forces and surface topography: Centimeter-scale spatial variation in wave forces. *Limnol. Oceanogr.,* **53**, 579–588, https://doi.org/10.4319/lo.2008.53.2.0579.

Reniers, A. J. H. M., J. H. MacMahan, F. Beron-Vera, and M. J. Olascoaga, 2010: Rip-current pulses tied to Lagrangian coherent structures. *Geophys. Res. Lett.,* **37**, https://doi.org/10.1029/2009GL041443.

Reniers, A. J. H. M., J. H. MacMahan, E. B. Thornton, T. P. Stanton, M. Henriquez, J. W. Brown, J. A. Brown, and E. Gallagher, 2009: Surf zone surface retention on a rip-channeled beach. *J. Geophys. Res.,* **114**, https://doi.org/10.1029/2008JC005153.

Shepard, F. P., and D. L. Inman, 1950: Nearshore water circulation related to bottom topography and wave refraction. *Eos Trans. AGU,* **31**, 196–212.

Shepard, F. P., K. O. Emery, and E. C. La Fond, 1941: Rip Currents: A Process of Geological Importance. *J. Geol.,* **49**, 337–369, https://doi.org/10.1086/624971.

Smith, J. A., J. L. Largier, 1995: Observations of nearshore circulation: Rip currents. *J. Geophys. Res.,* **100**, 10967–10975, https://doi.org/10.1029/95JC00751.

Sonu, C. J., 1972: Field observation of nearshore circulation and meandering currents. *Journal of Geophysical Research,* **77**, 3232–3247, https://doi.org/10.1029/JC077i018p03232.

Stephenson, W. J., L. E. Thornton, 2005: Australian Rock Coasts: review and prospects. *Aust. Geogr.,* **36**, 95–115, https://doi.org/10.1080/00049180500050946.

Sunamura, T., 2015: Rocky coast processes: With special reference to the recession of soft rock cliffs. *Proc. Jpn. Acad. Ser. B 9*, 481-500, https://doi.org/10.2183/pjab.91.481.

Trenhaile, A. S., 2002: Rock coasts, with particular emphasis on shore platforms. *Geomorphology,* **48**, 7–22, https://doi.org/10.1016/S0169-555X(02)00173-3.

Vagle, S., P. Chandler, and D. M. Farmer, 2005: On the dense bubble clouds and near bottom turbulence in the surf zone. *J. Geophys. Res.,* **110**, https://doi.org/10.1029/2004JC002603.

Velimirov, B., 1980: Formation and potential trophic significance of marine foam near kelp beds in the Benguela upwelling system. *Marine Biology,* **58**, 311–318.

Velimirov, B., J. Field, C. Griffiths, and P. Zoutendyk, 1977: The ecology of kelp bed communities in the Benguela upwelling system. *Helgoländer Wissenschaftliche Meeresuntersuchungen,* **30**, 495–518.

Winter, G., R. J. Lowe, G. Symonds, J. E. Hansen, and A. R. van Dongeren, 2017: Standing infragravity waves over an alongshore irregular rocky bathymetry. *J. Geophys. Res. Oceans,* **122**, 4868–4885, https://doi.org/10.1002/2016JC012242.

INITIAL DISTRIBUTION LIST

1. Defense Technical Information Center
   Ft. Belvoir, Virginia

2. Dudley Knox Library
   Naval Postgraduate School
   Monterey, California